

Comparison of speed loop control methods for IPM motor in electric vehicles

An Thi Hoai Thu Anh¹, Tran Van Nhu², Tran Trong Hieu¹

¹Department of Electrical Engineering, Faculty of Electrical-Electronic Engineering, University of Transport and Communications, Hanoi, Vietnam

²Department of Automotive Mechanical Engineering, University of Transport and Communications, Hanoi, Vietnam

Article Info

Article history:

Received Jul 4, 2024

Revised Sep 7, 2024

Accepted Sep 19, 2024

Keywords:

Backstepping method

EV

IPMSM

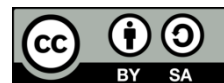
PI controller

Sliding mode control

ABSTRACT

With its outstanding features, such as high efficiency and torque-producing capability compared with the induction motor, the interior permanent magnet synchronous motor (IPMSM) has been increasingly researched and used for electric vehicles. The speed control strategy for both low and high speeds of the IPMSM is studied in conjunction with controllers based on the field-oriented control (FOC) structure to ensure accurate and stable system response under various operating conditions. This paper focuses on three control methods: sliding mode control (SMC), backstepping (BSP), and proportional integral (PI) for the speed loop to enhance system stability. Coupled with the presence of load disturbances, environmental disturbances, and uncertainties in parameters, comparisons and observations regarding the three methods can be made to conclude system stability and performance. Finally, simulation results on MATLAB/Simulink software confirm the effectiveness and validity of the proposed speed controllers.

This is an open access article under the [CC BY-SA](#) license.



Corresponding Author:

An Thi Hoai Thu Anh

Department of Electrical Engineering, Faculty of Electrical-Electronic Engineering

University of Transport and Communications

No. 3 Cau Giay, Lang Thuong Commune, Dong Da District, Hanoi, Vietnam

Email: htanh.ktd@utc.edu.vn

1. INTRODUCTION

Depleting fossil fuels and environmental pollution have become significant issues that any nation worldwide faces, which is partially attributable to means of transportation. Therefore, electric vehicles are currently considered a suitable solution to address these two issues. The interior permanent magnet synchronous motor (IPMSM) possesses advantages such as high efficiency, capability of generating ample torque, wide speed adjustment range, and high power density, making it an attractive choice in various fields such as electric vehicle manufacturing, wind power, aerospace, and widely applied in other industrial sectors [1]. When the motor operates at high speed, it is limited by voltage and energy, which may cause a decrease in output torque, current, and speed; the IPMSM can widen the speed adjustment range by controlling the torque in the weakening flux region [2]. To maximize the potential of this kind of motor, the maximum torque per ampere (MTPA) method is preferred [3], [4]. Widely used methods in IPMSM drives include direct torque control (DTC) and field-oriented control (FOC) [5]-[8], which are accompanied by various control methods and controllers applied to the speed loops. Conventional proportional integral (PI) controllers can control the motor [9], [10], but disturbances and changes in the motor's parameters have caused system instability. Nowadays, control theory is continuously evolving, and various control techniques have been widely utilized, such as sliding mode control (SMC), backstepping control, sliding mode variable structure

control (SMVSC), intelligent control, fuzzy control, neural networks, and adaptive control, which can operate IPMSM with high efficiency [11]-[20].

Dianov *et al.* [21] utilized the MTPA algorithm for the IPMSM drive system with PI controllers. Kirad *et al.* [22] applied sensorless backstepping technique with Kalman filtering to enhance motor performance. Feng *et al.* [23] developed a novel sliding mode control technology and comprehensive evaluation method for speed control of IPMSM to provide a rational assessment of speed control for synchronous PMSMs in various operating stages. Zhang *et al.* [24] designed and controlled field weakening of IPMSM for electric vehicles to demonstrate good dynamic performance and stable operation with the ability to extend speed up to four times the rated value. Belkacem *et al.* [25] compared backstepping sliding mode and reverse control for some vehicle components to demonstrate effectiveness and durability against external disturbances and different road conditions. Hosseini and Tabatabaei [26] controlled current and speed of IPMSM using segmented adaptive sliding mode control based on MTPA for current loop. Tung *et al.* [27] applied sliding mode observer for sensorless speed-controlled IPMSM with permanent magnet excitation along the axial magnetic field. Foo and Rahman [28] controlled MTPA in sensorless sliding mode for IPMSM drive system using sliding mode observer and high frequency (HF) signal transmission. Hashemi *et al.* [29] developed high-performance PI-based controllers for IPM motor drive system.

However, the existing studies have yet to propose and implement various control methods to replace PI and proportional integral derivative (PID) controllers for IPMSM motors operating in the field weakening region applicable to electric vehicles. Therefore, this paper will propose three different approaches to design controllers for the speed loop circuit applicable to electric cars, specifically VinFast electric vehicles. Finally, simulation results on MATLAB/Simulink software verified the correctness of the Authors' research.

2. MODELLING DRIVE SYSTEM OF ELECTRIC VEHICLES

2.1. Mathematical model of the IPMSM motor

The IPMSM model is represented in the d-q coordinate system as (1) [30]-[33]. Where $U_{sd}, U_{sq}, i_{sd}, i_{sq}$ are voltages, currents, resistance, inductances of the stator on dq-axis, ω_s is the angular velocity of the motor, ψ_p is the rotor flux, p_p is the number of pole pairs of the motor, T_e is the motor output torque, ψ_{sd}, ψ_{sq} are the stator flux on the dq-axis, T_L is the load torque, J is the moment of inertia of the motor, $T_{sd} = \frac{L_{sd}}{R_s}$ is the d-axis time constant of the stator circuit and $T_{sq} = \frac{L_{sq}}{R_s}$ is the q-axis time constant of the stator circuit.

$$\begin{cases} \frac{di_{sd}}{dt} = -\frac{1}{T_{sd}} i_{sd} + \omega_s \frac{L_{sq}}{L_{sd}} i_{sq} + \frac{1}{L_{sd}} U_{sd} \\ \frac{di_{sq}}{dt} = -\omega_s \frac{L_{sq}}{L_{sd}} i_{sd} - \frac{1}{T_{sq}} i_{sq} + \frac{1}{L_{sq}} U_{sq} - \omega_s \frac{\psi_p}{L_{sq}} \\ \psi_{sd} = L_{sd} i_{sd} + \psi_p \\ \psi_{sq} = L_{sq} i_{sq} \\ T_e = \frac{3}{2} p_p (\psi_p i_{sq} - i_{sd} i_{sq} (L_{sd} - L_{sq})) \\ T_e - T_L = \frac{J}{p_p} \frac{d\omega}{dt} \end{cases} \quad (1)$$

2.2. Modeling the forces acting on the electric vehicle

As the vehicle moves, the atmosphere will impede its motion. This resistance force consists the air resistance and the vehicle's friction with the air [34]. These two components combined form the wind resistance force, which is calculated by (2).

$$F_{wind} = \frac{1}{2} \rho C_d A_f (v_{veh} + v_{wind})^2 \quad (2)$$

Where ρ is the air density, C_d is the coefficient of air resistance (typically: $0.2 < C_d < 0.4$); A_f is the frontal area of the vehicle's body (cross-sectional area), and v_{wind} is the wind speed.

For rolling resistance, we only consider the rolling friction on a rigid road surface, and in the ideal case where all wheels have the same conditions, the rolling friction force can be calculated as (3) [5].

$$F_{roll} = f_r m_v g \cos \alpha \quad (3)$$

Where m_v is the total mass of the vehicle and passengers, g is the gravitational acceleration, α is the slope angle, f_r is the coefficient of rolling resistance calculated by (4). With v_{veh} being the velocity of the vehicle.

$$f_r = 0.01 \left(1 + \frac{3.6}{100} v_{veh} \right) \quad (4)$$

3. SPEED LOOP CONTROL DESIGN

Figure 1 presents the control structure based on the principle of field-oriented control on the dq -axis system to control the speed above the rated speed in the field weakening region. At the same time, the torque reaches the maximum value. The speed loop controllers are PI, backstepping, and sliding mode control to compare and evaluate the quality of speed control.

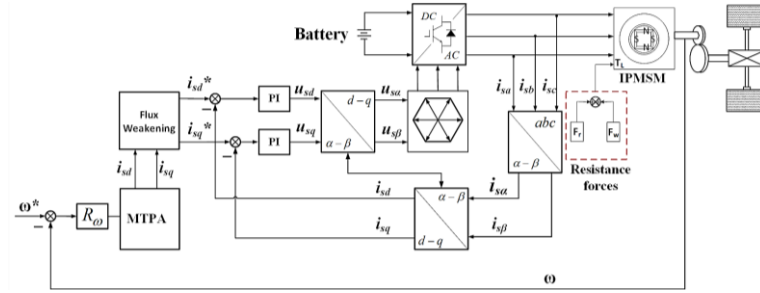


Figure 1. The field-oriented control structure of IPM

3.1. The sliding mode control design

Figure 2 shows the SMC controller structure, which defines the error between the desired and feedback angular velocity as (5), that $e = \omega - \omega^*$. Taking the derivative of the error as in (5).

$$\dot{e} = \dot{\omega} - \dot{\omega}^* = \frac{p_p}{J} (T_e - T_L) - \dot{\omega}^* \quad (5)$$

J is the moment of inertia, T_L is the load torque, p_p is the number of pole pairs. Choosing the Lyapunov function $V = \frac{1}{2} s^2$ [14]. The derivative of V is written as (6).

$$\dot{V} = s \cdot \dot{s} \quad (6)$$

To ensure stability conditions $\dot{V} < 0$, the sliding surface s is defined as follows: $s = e \Rightarrow \dot{s} = \dot{e}$. Setting $\dot{s} = 0$ we obtain the robust control component, as in (7).

$$T_e = \frac{-J}{p_p} \left(-\frac{p_p}{J} T_L - \dot{\omega}^* \right) \quad (7)$$

The system is stable when V is positive definite, continuously differentiable with first-order derivatives, and negative definite [35]. To ensure $s \cdot \dot{s} < 0$, the exponential reaching law is chosen to have the following form [36].

$$\dot{s} = -\varepsilon \operatorname{sgn}(s) - ks, \varepsilon > 0, k > 0 \quad (8)$$

Therefore, the control signal is designed as (9).

$$T_e = \frac{-J}{p_p} \left(ks - \frac{p_p}{J} T_L - \dot{\omega}^* + \varepsilon \operatorname{sgn}(s) \right) \quad (9)$$

With $k = 100$, $\varepsilon = 10$. Proving stability as (10).

$$\begin{aligned} \dot{V} &= s \cdot \dot{s} = \dot{e} = \dot{\omega} - \dot{\omega}^* = s \left[\frac{p_p}{J} (T_e - T_L) - \dot{\omega}^* \right] \\ &= s \left[\frac{p_p}{J} \left(\frac{-J}{p_p} \left(ks - \frac{p_p}{J} T_L - \dot{\omega}^* + \varepsilon \operatorname{sgn}(s) \right) - T_L \right) - \dot{\omega}^* \right] \\ &= s(-ks - \varepsilon \operatorname{sgn}(s)) = -(\varepsilon |s| + ks^2) \leq 0 \end{aligned} \quad (10)$$

3.2. The backstepping control design

Figure 3 shows the BSP controller structure. Let's define the error signal as: $e = \omega - \omega^*$, taking the derivative of both sides as in (11).

$$\dot{e} = \dot{\omega} - \dot{\omega}^* = \frac{p_p}{J}(T_e - T_L) - \dot{\omega}^* \quad (11)$$

Choosing the Lyapunov function $V = \frac{1}{2}e^2$. Taking the derivative of V [1]: $\dot{V} = e \cdot \dot{e}$. Choosing the control parameter $k > 0$ such as (12).

$$\dot{e} = -ke \Rightarrow \dot{V} = e \cdot (-ke) = -ke^2 < 0 \quad (12)$$

Substituting $\dot{e} = -ke$ into (11), we obtain (13). With $k = 100$.

$$\frac{p_p}{J}(T_e - T_L) - \dot{\omega}^* = -ke \Rightarrow T_e = T_L - \frac{J}{p_p}(ke - \dot{\omega}^*) \quad (13)$$

3.3. The PI controller design

When synthesizing the speed loop circuit, as shown in Figure 4, we consider the entire current loop as a function of the optimal module standard and regard the component $(L_{sd} - L_{sq})i_{sd}i_{sq}$ as noise [37]-[39]. The speed control loop with the transfer function, as (14).

$$P = \frac{1}{K_i(1+2T_{si}p+2T_{si}^2p^2)} \cdot \frac{3p_p\psi_p}{2} \cdot \frac{K_\omega}{T_\omega p+1} \quad (14)$$

With $T_{si} = 2T_i$. According to the optimal module standard, select the normalized function, as (15).

$$F_c = \frac{1}{2T^2\sigma s^2 + 2T\sigma s + 1} \quad (15)$$

Set $K = 2K_i/(3p_c\psi_p)$. The controller is as (16).

$$R_\omega = \frac{F_c}{(1-F_c)P} = \frac{(1+2T_{si}p+2T_{si}^2p^2) \cdot K \cdot (1+T_\omega p) \cdot Jp}{2p_cK_\omega(1+T_\sigma p)T_\sigma p} \quad (16)$$

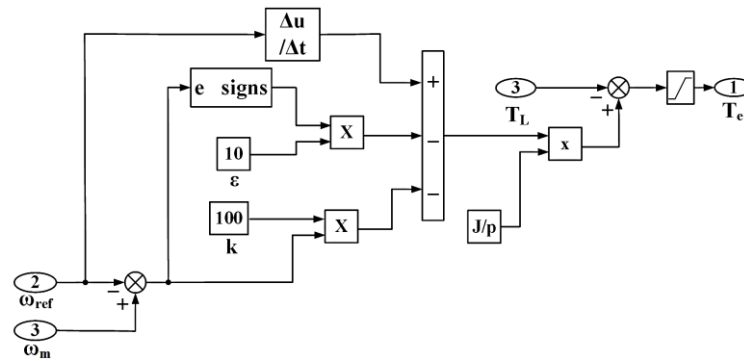


Figure 2. SMC controller structure

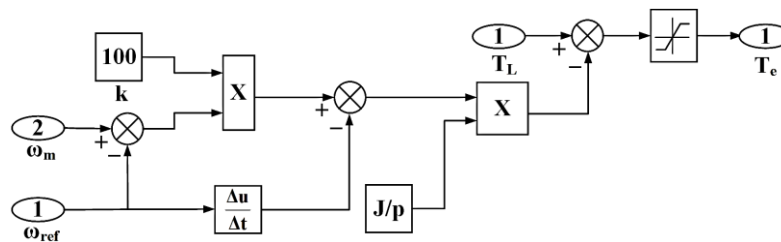


Figure 3. BSP controller structure

Eliminate high-order components, as (17).

$$R_\omega = \frac{(1+2T_{si}p).K.(1+T_\omega p).Jp}{2p_p K_\omega (1+T_\sigma p) T_\sigma p} = \frac{[1+(2T_{si}+T_\omega)].K.Jp}{2p_p K_\omega (1+T_\sigma p) T_\sigma p} \quad (17)$$

Deselect: $T_\sigma = T_{s\omega} = 2T_{si} + T_\omega$; We have $R_\omega = \frac{K.Jp}{2p_c K_\omega T_{s\omega} p}$.

The controller becomes a simple stage incapable of eliminating static error while there is load disturbance. The symmetric optimal synthesis method can overcome this drawback. Choosing the standard function according to symmetric optimization as (18).

$$F_c = \frac{1+4T_\sigma p}{1+4T_\sigma p+8T^2_\sigma p^2+8T^3_\sigma p^3} \quad (18)$$

Where $R_\omega = \frac{F_c}{(1-F_c)p}$ and setting $T_\sigma = T_{s\omega} = 2T_{si} + T_\omega$

From there, we obtain (19).

$$R_\omega = \frac{F_c}{(1-F_c)p} = \frac{(1+2T_{si}p+2T^2_{si}p^2).K.(1+T_\omega p)(1+4T_\sigma p).Jp}{8p_p K_\omega (1+T_\sigma p) T^2_\sigma p^2} \quad (19)$$

Eliminating the high-order terms with (20).

$$R_\omega = \frac{(1+2T_{si}p).K.(1+T_\omega p)(1+4T_\sigma p).Jp}{8p_p K_\omega (1+T_\sigma p) T^2_\sigma p^2} = \frac{[1+(2T_{si}+T_\omega)p].K.(1+4T_\sigma p).J}{8p_p K_\omega (1+T_\sigma p) T^2_\sigma p} = \frac{K.(1+4T_\sigma p).J}{8p_p K_\omega T^2_\sigma p} \quad (20)$$

Obtaining the speed controller as (21).

$$R_\omega = \frac{K.J}{2p_p K_\omega T_{s\omega}} \left(1 + \frac{1}{4.T_{s\omega}.p}\right) \quad (21)$$

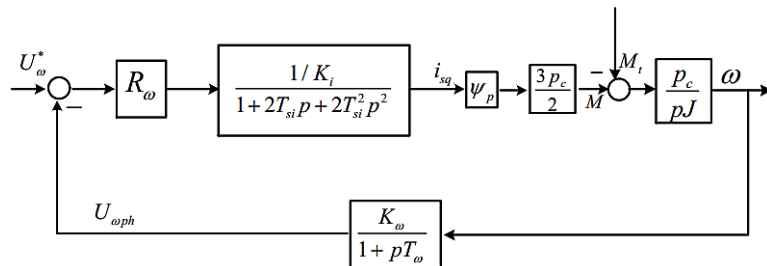


Figure 4. Speed loop circuit

4. SIMULATION RESULTS

The theoretical studies validated through responses simulated on MATLAB software include three control methods for the speed loop of the FOC structure applied in electric vehicles. The responses are implemented in MATLAB/ Simulink using the simulation parameters from Tables 1 and 2. The speed profile is based on Europe ECE's standard urban cycle [40]. The speed response of the electric vehicle transmission control system using PI, BSP, and SMC is illustrated in Figure 5. Figure 5 compares the speed response results of three methods: PI, BSP, and SMC. SMC and BSP demonstrate relatively short transient response times of about 0.07 s, whereas PI responds slower, around 0.2 s. Moreover, during the transition from acceleration to steady-state, an overshoot occurred. From Figure 5, we can observe that the overshoot of PI is the largest, leading to oscillation and a more extended response time, followed by BSP and, finally, SMC.

The three control methods, PI, BSP, and SMC, have been conducted when the load changes, and the results are presented in Figure 6. Overall, when operating at speeds higher than the rated speed (1200 rpm), all three methods show a decrease in electromagnetic torque to increase the speed. This leads to a higher peak value of the torque oscillation in the PI method and a larger amplitude of oscillation, potentially affecting the system's stability. Conversely, we observe a smaller peak value of the electromagnetic torque oscillation in SMC, with a lower amplitude of oscillation and smaller torque. This result indicates that the system is less affected by load disturbances.

Figure 7 illustrates the waveforms of i_{sd} and i_{sq} . Looking at Figure 7(a), we can observe that the two currents i_{sd} and i_{sq} have been decoupled, with i_{sd} being controlled to be less than 0. Examining Figure 7(b) and Figure 7(c), during sudden load changes in PI and BSP control, i_{sd} and i_{sq} currents oscillate and exhibit more giant spikes, affecting the system's stability. In contrast, SMC exhibits more minor oscillations, providing better response and being less affected by load changes.

Table 1. Parameters of motor IPM

Parameters	Symbol	Value	Unit
Stator resistance	R_s	0.0065	Ohm
d-axis inductance	L_{sd}	0.001597	H
q-axis inductance	L_{sq}	0.002057	H
Inertia torque	J	0.09	kg.m ²
Number of pole pairs	p_p	3	
DC voltage	V_{dc}	550	V

Table 2. Parameters of an electric car

Parameters	Value	Unit
Vehicle weight + load	2018	kg
Wheel radius	0.3	m
Transmission ratio	9.73	
Maximum speed	130	km/h
Effective area	2.3	m ²
Air density	1.25	kg/m ³
Road gradient	0	
Rolling resistance coefficient	0.02	

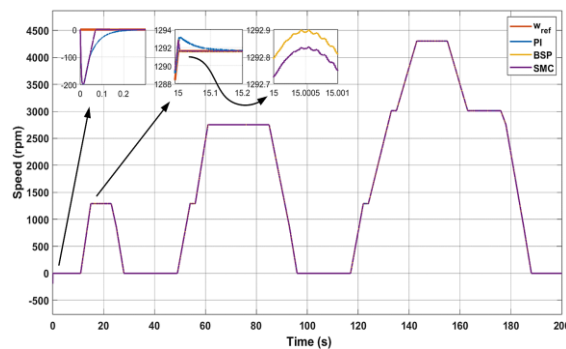


Figure 5. The speed response

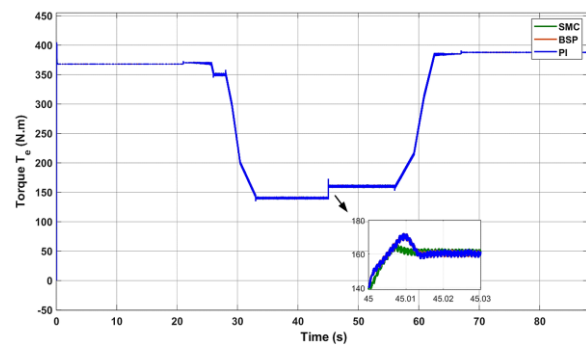


Figure 6. Torque response as load changes

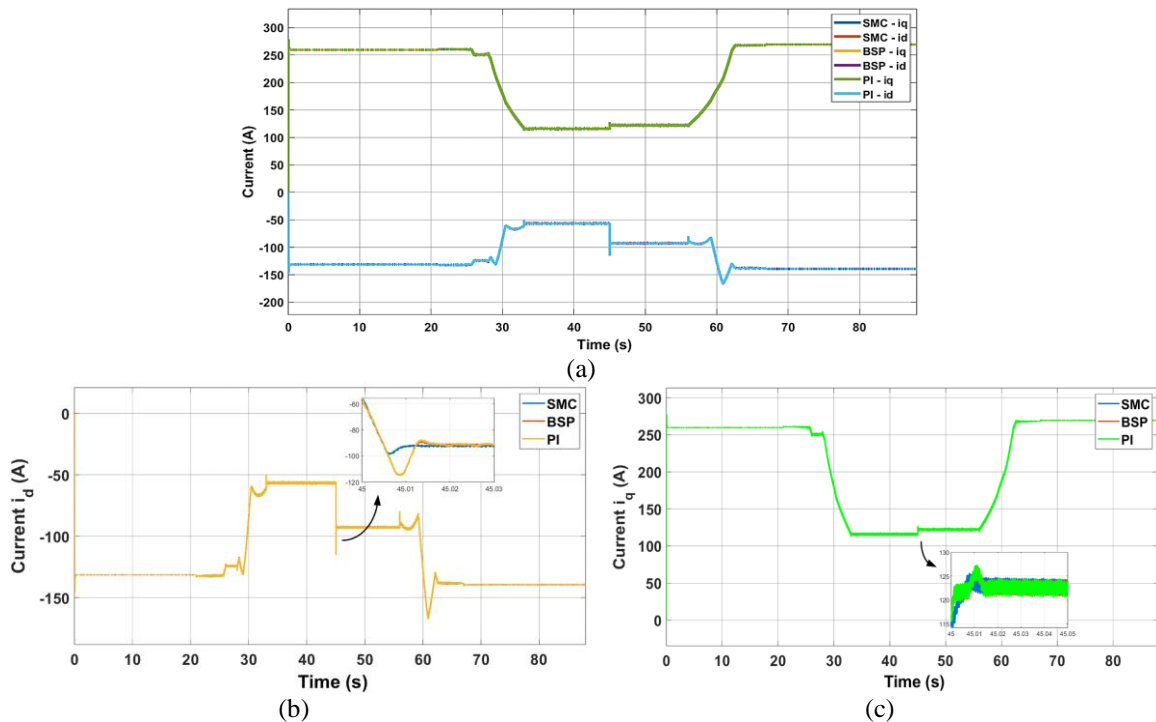


Figure 7. Current response to sudden load changes: (a) comparison of the current responses i_{sd} and i_{sq} of three methods, (b) zoom out i_{sd} , and (c) zoom out i_{sq}

5. CONCLUSION

This paper has presented a comparison of three control methods, PI, SMC, and BSP, for the speed control loop of the IPM motor to evaluate them based on criteria such as stability, response time, and accuracy in speed control even when the load changes. Simulation results have shown that the sliding mode control (SMC) method yielded the best results among the three compared methods. SMC ensures high stability and fast response time and minimizes control errors, especially under dynamic and noisy conditions while the overshoot of PI is the largest, leading to oscillation and more extended response time; PI and BSP cause i_{sd} and i_{sq} currents to oscillate as load changes. These results suggest that SMC can be effectively applied in IPM control systems, particularly when high precision and fast response are required. This research provides a foundation for selecting the appropriate control method in IPM motor control applications.

FUNDING INFORMATION

Authors state no funding is involved.

AUTHOR CONTRIBUTIONS STATEMENT

This journal uses the Contributor Roles Taxonomy (CRediT) to recognize individual author contributions, reduce authorship disputes, and facilitate collaboration.

Name of Author	C	M	So	Va	Fo	I	R	D	O	E	Vi	Su	P	Fu
An Thi Hoai Thu Anh	✓	✓	✓	✓	✓	✓		✓	✓	✓		✓	✓	✓
Tran Van Nhu		✓				✓	✓		✓		✓			
Tran Trong Hieu			✓			✓	✓	✓		✓	✓		✓	

C : **C**onceptualization

M : **M**ethodology

So : **S**oftware

Va : **V**alidation

Fo : **F**ormal analysis

I : **I**nterpretation

R : **R**esources

D : **D**ata Curation

O : **O**riginal Draft

E : **E**diting

Vi : **V**isualization

Su : **S**upervision

P : **P**roject administration

Fu : **F**unding acquisition

CONFLICT OF INTEREST STATEMENT

Authors state no conflict of interest

DATA AVAILABILITY

The data that support the findings of this study are openly available in IJPEDS at DOI: 10.11591/ijpeds.v15.i4.ppab-cd.

REFERENCES




- [1] M. A. Hamida, J. de Leon, and A. Glumineau, "Experimental sensorless control for IPMSM by using integral backstepping strategy and adaptive high gain observer," *Control Engineering Practice*, vol. 59, pp. 64–76, Feb. 2017, doi: 10.1016/j.conengprac.2016.11.012.
- [2] Z. Xinghua, T. Qitai, and W. Ting, "Direct torque control of interior permanent magnet synchronous motor with maximum torque per ampere," in *2016 IEEE 11th Conference on Industrial Electronics and Applications (ICIEA)*, IEEE, Jun. 2016, pp. 1519–1524, doi: 10.1109/ICIEA.2016.7603826.
- [3] C. Mademlis and V. G. Agelidis, "On considering magnetic saturation with maximum torque to current control in interior permanent magnet synchronous motor drives," *IEEE Transactions on Energy Conversion*, vol. 16, no. 3, pp. 246–252, 2001, doi: 10.1109/60.937204.
- [4] S. Jin, W. Jin, H. Wang, S. Yu, and Z. Zhang, "Maximum torque per ampere control of permanent magnet/reluctance hybrid rotor dual stator synchronous motor," *IET Electric Power Applications*, vol. 18, no. 9, pp. 1021–1032, Sep. 2024, doi: 10.1049/elp2.12453.
- [5] B. K. Bose, "Modern power electronics and AC drives," *Prentice Hall PTR*, vol. 81, no. 17, p. 411, 1974.
- [6] N. P. Quang and J.-A. Dittrich, *Vector control of three-phase AC machines*, 2nd ed. Berlin, Heidelberg, 2008. doi: 10.1007/978-3-540-79029-7.
- [7] A. Ghamri, R. Boumaaraf, M. T. Benchouia, H. Mesloub, A. Goléa, and N. Goléa, "Comparative study of ANN DTC and conventional DTC controlled PMSM motor," *Mathematics and Computers in Simulation*, vol. 167, pp. 219–230, Jan. 2020, doi: 10.1016/j.matcom.2019.09.006.
- [8] Z. Jia and B. Kim, "Online trained neural network-PI speed controller for DTC based IPMSM drives," *International Journal of Electrical and Electronic Engineering & Telecommunications*, vol. 7, no. 3, pp. 108–113, 2018, doi: 10.18178/ijeetc.7.3.108-113.
- [9] A. K. Singh and O. P. Roy, "Performance analysis of a PMSM drive using PID controllers," *Electronics Information and Planning*, vol. 37, no. 3, pp. 80–87, 2010.

- [10] L. Wang, K. Xiao, L. de Lillo, L. Empringham, and P. Wheeler, "PI controller relay auto-tuning using delay and phase margin in PMSM drives," *Chinese Journal of Aeronautics*, vol. 27, no. 6, pp. 1527–1537, Dec. 2014, doi: 10.1016/j.cja.2014.10.019.
- [11] Z. Song, X. Mei, T. Tao, and M. Xu, "The sliding-mode control based on a novel reaching technique for permanent magnet synchronous motors," *Electric Power Components and Systems*, vol. 47, no. 16–17, pp. 1505–1513, Oct. 2019, doi: 10.1080/15325008.2019.1663299.
- [12] P. Hou, X. Wang, and Y. Sheng, "Research on flux-weakening control system of interior permanent magnet synchronous motor based on fuzzy sliding mode control," *Proceedings of the 31st Chinese Control and Decision Conference, CCDC 2019*, pp. 3151–3156, 2019, doi: 10.1109/CCDC.2019.8832483.
- [13] A. A. A. Samat, M. N. Fazli, N. A. Salim, A. M. S. Omar, and M. K. Osman, "Speed control design of permanent magnet synchronous motor using Takagi- Sugeno fuzzy logic control," *Journal of Electrical Systems*, vol. 13, no. 4, pp. 689–695, 2017.
- [14] A. Jaffar Sadiq Ali and G. P. Ramesh, "Neural network-controlled wind generator-fed r-Z source-based PMSM drive," *Advances in Intelligent Systems and Computing*, vol. 517, pp. 387–396, 2017, doi: 10.1007/978-981-10-3174-8_34.
- [15] M. M. Seddik and B. A. Essalam, "Nonlinear control of the permanent magnet synchronous motor PMSM using input-output linearization control and sliding mode control," *Studies in Engineering and Exact Sciences*, vol. 5, no. 2, p. e9156, Oct. 2024, doi: 10.54021/seesv5n2-333.
- [16] Z. Lan, F. Shen, G. Zhu, C. Chen, L. Li, and C. Cao, "A novel control method of improved flux-weakening trajectory for IPMSM," in *2019 22nd International Conference on Electrical Machines and Systems (ICEMS)*, IEEE, Aug. 2019, pp. 1–6. doi: 10.1109/ICEMS.2019.8921440.
- [17] F. Liu, H. Li, L. Liu, R. Zou, and K. Liu, "A control method for IPMSM based on active disturbance rejection control and model predictive control," *Mathematics*, vol. 9, no. 7, p. 760, Apr. 2021, doi: 10.3390/math9070760.
- [18] R. Trabelsi, A. Kheder, M. F. Mimouni, and F. M'sahli, "Backstepping control for an induction motor with an adaptive Backstepping rotor flux observer," in *18th Mediterranean Conference on Control and Automation, MED'10*, IEEE, Jun. 2010, pp. 5–10. doi: 10.1109/MED.2010.5547625.
- [19] M. A. Iqbal and A. Y. Memon, "Robust backstepping sensorless speed control of PMSM using cascaded sliding mode and high gain observers," in *2019 International Symposium on Recent Advances in Electrical Engineering (RAEE)*, IEEE, Aug. 2019, pp. 1–6. doi: 10.1109/RAEE.2019.8886948.
- [20] M. A. Hamida, A. Glumineau, and J. De Leon, "High order sliding mode controller and observer for sensorless IPM synchronous motor," *International Conference on Power Engineering, Energy and Electrical Drives*, pp. 955–960, 2013, doi: 10.1109/PowerEng.2013.6635739.
- [21] A. Dianov, Kim Young-Kwan, Lee Sang-Joon, and Lee Sang-Taek, "Robust self-tuning MTPA algorithm for IPMSM drives," in *2008 34th Annual Conference of IEEE Industrial Electronics*, IEEE, Nov. 2008, pp. 1355–1360. doi: 10.1109/IECON.2008.4758151.
- [22] A. Kirad, S. Grouni, and Y. Soufi, "Improved sensorless backstepping controller using extended Kalman filter of a permanent magnet synchronous machine," *Bulletin of Electrical Engineering and Informatics*, vol. 11, no. 2, pp. 658–671, 2022, doi: 10.11591/eei.v11i2.3560.
- [23] L. Feng, M. Deng, S. Xu, and D. Huang, "Speed regulation for PMSM drives based on a novel sliding mode controller," *IEEE Access*, vol. 8, pp. 63577–63584, 2020, doi: 10.1109/ACCESS.2020.2983898.
- [24] Y. Zhang, W. Cao, S. McLoone, and J. Morrow, "Design and flux-weakening control of an interior permanent magnet synchronous motor for electric vehicles," *IEEE Transactions on Applied Superconductivity*, vol. 26, no. 7, pp. 1–6, 2016, doi: 10.1109/TASC.2016.2594863.
- [25] M. Belkacem, K. Z. Meguenni, and I. K. Bousserhane, "Comparative study between backstepping and backstepping sliding mode controller for suspension of vehicle with a magneto-rheological damper," *International Journal of Power Electronics and Drive Systems*, vol. 13, no. 2, pp. 689–704, 2022, doi: 10.11591/ijpeds.v13.i2.pp689-704.
- [26] S. H. Hosseini and M. Tabatabaei, "IPMSM velocity and current control using MTPA based adaptive fractional order sliding mode controller," *Engineering Science and Technology, an International Journal*, vol. 20, no. 3, pp. 896–908, 2017, doi: 10.1016/j.jestch.2017.03.008.
- [27] N. M. Tung, Q. D  ng, H. Ph  ng, Q. D  i, and L. D  r, "Sensorless speed control of axial gap permanent magnet motor using sliding mode observer," *Measurement, Control, and Automation*, vol. 3, no. 1, pp. 23–29, 2022.
- [28] G. Foo and M. F. Rahman, "Sensorless sliding-mode MTPA control of an IPM synchronous motor drive using a sliding-mode observer and HF signal injection," *IEEE Transactions on Industrial Electronics*, vol. 57, no. 4, pp. 1270–1278, 2009, doi: 10.1109/TIE.2009.2030820.
- [29] Z. Hashemi, M. Mardaneh, and M. Sha Sadeghi, "High performance controller for interior permanent magnet synchronous motor drive using artificial intelligence methods," *Scientia Iranica*, vol. 19, no. 6, pp. 1788–1793, 2012, doi: 10.1016/j.scient.2012.07.001.
- [30] Z. Zhang and X. Liu, "A duty ratio control strategy to reduce both torque and flux ripples of DTC for permanent magnet synchronous machines," *IEEE Access*, vol. 7, pp. 11820–11828, 2019, doi: 10.1109/ACCESS.2019.2892121.
- [31] H. Wang, C. Li, G. Zhang, Q. Geng, and T. Shi, "Maximum torque per ampere (MTPA) control of IPMSM systems based on controller parameters self-modification," *IEEE Transactions on Vehicular Technology*, vol. 69, no. 3, pp. 2613–2620, 2020, doi: 10.1109/TVT.2020.2968133.
- [32] K. Zhao *et al.*, "Sliding mode-based velocity and torque controllers for permanent magnet synchronous motor drives system," *The Journal of Engineering*, vol. 2019, no. 23, pp. 8604–8608, Dec. 2019, doi: 10.1049/joe.2018.9065.
- [33] S. Rebouh, A. Kaddouri, R. Abdessemed, and A. Haddoun, "Adaptive backstepping speed control for a permanent magnet synchronous motor," in *2011 International Conference on Management and Service Science*, IEEE, Aug. 2011, pp. 1–4. doi: 10.1109/ICMSS.2011.5999372.
- [34] X. Zhang and C. Mi, "Vehicle power management: modeling, control and optimization," *Power Systems*, vol. 51, 2011, doi: 10.1007/978-0-85729-736-5.
- [35] F. Mohd Zaihidee, S. Mekhilef, and M. Mubin, "Robust speed control of PMSM using sliding mode control (SMC)—A review," *Energies*, vol. 12, no. 9, p. 1669, May 2019, doi: 10.3390/en12091669.
- [36] J. Liu and X. Wang, "Advanced sliding mode control," *Advanced Sliding Mode Control for Mechanical Systems*, pp. 81–96, 2011, doi: 10.1007/978-3-642-20907-9_3.
- [37] Y. Zafari, A. H. Mazinan, and S. Shoja-Majidabad, "Speed control of five-phase IPMSM through PI, SMC and FITSMC approaches under normal and open phase faulty conditions," *Automatika*, vol. 58, no. 4, pp. 506–519, Oct. 2017, doi: 10.1080/00051144.2018.1478928.




- [38] H. Ben Achour, S. Ziani, Y. Chaou, Y. El Hassouani, and A. Daoudia, "Permanent magnet synchronous motor PMSM control by combining vector and PI controller," *WSEAS Transactions on Systems and Control*, vol. 17, pp. 244–249, May 2022, doi: 10.37394/23203.2022.17.28.
- [39] A. Apte, U. Thakar, and V. Joshi, "Disturbance observer based speed control of PMSM using fractional order PI controller," *IEEE/CAA Journal of Automatica Sinica*, vol. 6, no. 1, pp. 316–326, Jan. 2019, doi: 10.1109/JAS.2019.1911354.
- [40] T. Barlow, S. Latham, I. McCrae, and P. Boulter, "A reference book of driving cycles for use in the measurement of road vehicle emissions," *TRL Published Project Report*, p. 280, 2009, [Online]. Available: http://www.trl.co.uk/online_store/reports_publications/trl_reports/cat_traffic_and_the_environment/report_a_reference_book_of_driving_cycles_for_use_in_the_measurement_of_road_vehicle_emissions.htm%5Chttps://www.gov.uk/government/uploads/system/uploads/a

BIOGRAPHIES OF AUTHORS






An Thi Hoai Thu Anh    received her Engineer (1997) and M.Sc. (2002) degrees in Industrial Automation Engineering from Hanoi University of Science and Technology; and completed Ph.D. degree in 2020 from University of Transport and Communications (UTC). Now, she is a lecturer at the Faculty of Electrical and Electronic Engineering at the University of Transport and Communications (UTC). Her current interests include power electronic converter, electric motor drive control, and energy-saving solutions applied to industry and transportation. She can be contacted at email: htanh.ktd@utc.edu.vn.



Tran Van Nhu    received his Engineer and M.Sc. degrees in Mechanical Engineering from the University of Transport and Communications in 2001 and 2007, respectively. In 2009, he was also awarded a Ph.D. degree in Mechanical Engineering from the Polytechnic University of Huts-de-France, France. He currently holds a lecturer-researcher position at the Faculty of Mechanical Engineering, University of Transport and Communications. His research is focused on vehicle dynamics and control and quasi-LPV systems. He can be contacted at email: vannhu.tran@utc.edu.vn.



Tran Trong Hieu    is a fourth-year student majoring in Electrical Engineering at the University of Transport and Communications (UTC), Vietnam. His current interests include power electronics control and electric drive control, which are applied in the transportation and industry. He can be contacted at email: hieu2k2boha@gmail.com.